Growth and Properties of Semiconductor Core/Shell Nanocrystals with InAs Cores

YunWei Cao and Uri Banin*

Contribution from the Department of Physical Chemistry, and the Farkas Center for Light Induced Processes, The Hebrew University, Jerusalem 91904, Israel

Received April 19, 2000

Abstract: Core/shell semiconductor nanocrystals with InAs cores were synthesized and characterized. III−V semiconductor shells (InP and GaAs), and II−VI semiconductor shells (CdSe, ZnSe, and ZnS) were overgrown on InAs cores with various radii using a two step synthesis. In the first step cores were prepared, and in the second step the shells were grown using high-temperature pyrolysis of organometallic precursors in a coordinating solvent. Core/shell growth was monitored by absorption and photoluminescence spectroscopy. The band gap shifts to the red upon growth of InP or CdSe shells, while for ZnSe and ZnS shells that have larger band offsets with respect to InAs, the band gap energy is maintained. This behavior is reproduced by band gap energy calculations using a particle within a spherical box model. The photoluminescence quantum yield is quenched in InAs/InP core/shells but increases substantially up to 20% for InAs/CdSe and InAs/ZnSe core/shells. For InAs/ZnS core/shells the enhancement of the photoluminescence quantum yields is smaller, up to 8%. The core/shell nanocrystals were characterized using transmission electron microscopy, X-ray photoelectron spectroscopy, and powder X-ray diffraction. X-ray photoelectron spectroscopy provides evidence for shell growth. The X-ray diffraction peaks shift and narrow upon shell growth, providing evidence for an epitaxial growth mode. Simulations of the X-ray diffraction patterns reproduce both effects, and show that there is one stacking fault present for every four to five layers in the core and core/shell nanocrystals. The stability of InAs/CdSe and InAs/ZnSe core/shells against oxidation is substantially improved compared with the cores, and the photostability is significantly better compared with a typical near-IR laser dye IR140. Core/shell nanocrystals with InAs cores are suggested as a novel type of fluorophores covering the near-IR spectral range, with high emission quantum yields and improved stability compared with traditional near-IR laser dyes.

Introduction

The emission color from semiconductor nanocrystal quantum dots is tunable by the size as a result of the quantum-confinement effect.[1−4] Harnessing this emission for real-world applications such as biological fluorescence marking[5−7] and optoelectronic devices[8−11] is an important challenge, which imposes stringent requirements of a high fluorescence quantum yield (QY), and of stability against photodegradation. These characteristics are difficult to achieve in semiconductor nanocrystals coated by organic ligands due to imperfect surface passivation. In addition, the organic ligands are labile for exchange reactions because of their weak bonding to the nanocrystal surface atoms.[12] A proven strategy for increasing both the fluorescence QY and the stability, is to grow a shell of a higher band gap semiconductor on the core nanocrystal.[13−20] In such composite core/shell structures, the shell type and shell thickness, provide further control for tailoring the optical, electronic, electrical, and chemical properties of semiconductor nanocrystals. We report on the high-temperature colloidal growth of various III−V and II−VI semiconductor shells on InAs core nanocrystals. The chemistry and properties of these novel core/shell semiconductor nanocrystals are investigated with the goal of obtaining fundamental insights into the mechanisms and the limitations of solution-phase epitaxial growth. The band gap energy of these core/shell nanocrystals is tunable in the near-IR (NIR) spectral range, covering the

* To whom correspondence should be addressed. E-mail: banin@chem.ch.huji.ac.il.

(1) Nirmal, M.; Brus, L. *Acc. Chem. Res.* **1999**, *32*, 407.
(2) Alivisatos, A. P. *Science* **1996**, *271*, 933.
(3) Weller, H. *Angew. Chem.. Int. Ed. Engl*. **1993**, *32*, 41.
(4) Banin, U.; Cao, Y. W.; Katz, D.; Millo, O. *Nature* **1999**, 400, 542.
(5) Bruchez, M.; Moronne, M.; Gin, P.; Weiss, S.; Alivisatos, A. P. *Science* **1998**, *281*, 2013.
(6) Chan, W. C. W.; Nie, S. *Science* **1998**, *281*, 2016.
(7) Mitchell, G. P.; Mirkin, C. A.; Letsinger, R. L. *J. Am. Chem. Soc.* **1999**, *121*, 8122.
(8) Colvin, V. L.; Schlamp, M. C.; and Alivisatos, A. P. *Nature* **1994**, *370*, 354.
(9) Dabboussi, B. O.; Bawendi, M. G.; Onitsuka, O.; and Rubner, M. F. *Appl. Phys. Lett.* **1995**, *66*, 1316.
(10) Schlamp, M. C.; Peng, X. G.; Alivisatos, A. P. *J. Appl. Phys.* **1997**, *82*, 5837.
(11) Mattoussi, H.; Radzilowski, L. H.; Dabbousi, B. O.; Thomas, E. L.; Bawendi, M. G.; Rubner, M. F. *J. Appl. Phys.* **1998**, *83*, 7965.
(12) Kuno, M.; Lee, J. K.; Dabbousi B. O.; Mikulec, F. V.; Bawendi, M. G. *J. Chem. Phys.* **1997**, *106*, 9869.
(13) Mews, A.; Eychmüller, A.; Giersig, M.; Schoos, D.; Weller, H. *J. Phys. Chem.* **1994**, *98*, 934.
(14) Hines, M. A.; Guyot-Sionnest, P. J. *J. Phys. Chem.* **1996**, *100*, 468.
(15) Peng, X.; Schlamp, M. C.; Kadavanich, A. V.; Alivisatos, A. P. *J. Am. Chem. Soc.* **1997**, *119*, 7019.
(16) Dabbousi, B. O.; Rodriguez-Viejo, J.; Mikulec, F. V.; Heine, J. R.; Mattoussi, H.; Ober, R.; Jensen, K. F.; Bawendi, M. G. *J. Phys. Chem. B* **1997**, *101*, 9463.
(17) Tian, Y.; Newton, T.; Kotov, N. A.; Guldi, D. M.; Fendler, J. H. *J. Phys. Chem.* **1996**, *100*, 8927.
(18) Cao, Y. W., and Banin, U. *Angew.Chem., Int. Ed.* **1999**, *38*, 3692.
(19) Kershaw, S. V.; Burt, M.; Harrison, M.; Rogach, A.; Weller, H.; Eychmuller, A. *Appl. Phys. Lett.* **1999**, *75*, 1694.
(20) Harrison, M. T.; Kershaw, S. V.; Rogach, A. L.; Kornowski, A.; Eychmuller, A.; Weller, H. *Adv. Mater.* **2000**, *12*, 123.

10.1021/ja001386g CCC: $19.00 © 2000 American Chemical Society
Published on Web 09/21/2000

wavelengths that are important for telecommunication applications. These core/shell nanocrystals may be further developed to serve as efficient fluorescent labels for biological applications in the NIR range.[21]

The colloidal chemical route is widely applicable for synthesis of a variety of II−VI semiconductor nanocrystals such as CdSe,[22] as well as for III−V semiconductors such as InP[23−25] and InAs.[26] Of particular relevance to the present work is the preparation of high quality InAs nanocrystals, by a solution pyrolytic reaction of organometallic precursors in trioctylphosphine (TOP).[27] Band gap fluorescence, tunable between 800 and 1400 nm for radii ranging between 1 and 4 nm respectively, is observed, but the QY at room temperature is limited to 0.5−2%.[26,28] The limited QY is related to the surface passivation of the nanocrystals, which are overcoated by TOP ligands. TOP is a Lewis base that preferentially binds to cationic indium sites on the surface. This, along with the steric hindrance that the bulky TOP ligands impose on neighboring nanocrystal surface sites, leads to incomplete electronic passivation of surface dangling orbitals. The presence of such sites provides efficient pathways for nonradiative decay of the nanocrystal excited state, thus limiting the maximum fluorescence QY. In II−VI semiconductor nanocrystals, core/shell structures were developed to overcome these limitations of organic passivation of the surface, beginning with the successful synthesis of highly emitting CdSe/ZnS nanocrystals by Guyot-Sionnest and co-workers.[14] The synthesis of CdSe/ZnS core/shells employs a high-temperature route in TOP/TOPO solution (TOPO is trioctylphosphineoxide).[14,16] Another approach employed a low-temperature route to grow CdSe/CdS core/shells in pyridine.[15] These core/shell nanocrystals fluoresce in the visible range with a QY of 30−90% and have increased photochemical stability.

The core/shell approach is conceptually closely related to the approach used in two-dimensional quantum wells.[29] In a quantum well, a thin layer of nanometric dimensions of a low band gap semiconductor, is sandwiched between thick layers of a high band gap semiconductor, forming a square potential well for the electron and hole wave functions. The determining factor for growth of quantum wells is the lattice mismatch between the two semiconductors. The electronic properties of the quantum well are determined primarily by the energetic offsets between the conduction and valence band edges of the two semiconductors. We have examined the influence of the lattice mismatch and the band offsets on the growth and electronic properties of core/shell nanocrystals with InAs cores. In Figure 1 we show schematically the values of both parameters for InAs and the variety of shell materials that we investigated.[30] The lattice mismatch ranges from nearly zero for CdSe shells, to as high as 10.7% for ZnS shells. The band offsets cover a broad range of values as well. Note that the shell materials include both II−VI and III−V semiconductors, a selection that provides substantial tunability for the properties of the composite core/shell nanocrystals.

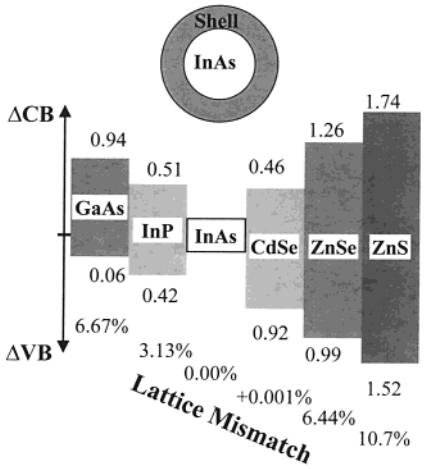

Figure 1. Summary of the band offsets (in eV) and lattice mismatch (in %) between the core InAs and the III−V semiconductor shells (left side), and II−VI semiconductor shells (right side) grown in this work. CB = conduction band; VB = valence band.

In a recent contribution, we reported on the growth of InAs/InP and InAs/CdSe core/shells, two shell materials with similar conduction band offsets relative to InAs.[18] The growth of CdSe shells resulted in an impressive 20-fold enhancement of the room-temperature QY, up to levels better than traditional organic NIR laser dyes. Here, we report on a complete characterization of these core/shells, as well as on the development of new core/shells—InAs/ZnSe and InAs/ZnS. In these latter cases there are large band offsets between the core and shell semiconductors. We have grown shells of the various semiconductors on InAs cores with different diameters, in particular, a size with fluorescence at 1.3 μm, a wavelength suited for fiber-optic communications.[31] The detailed characterization of all the core/shells is described.

Experimental Section

A. Synthesis of Core/Shell Nanocrystals. 1. Chemicals. Gallium(III) chloride ($GaCl_3$), indium(III) chloride ($InCl_3$), tris(tri-methylsilyl) phosphide {$(TMS)_3P$}, dimethylcadmium ($Cd(CH_3)_2$) were purchased from Strem and used without further purification. Trioctylphosphine (TOP, 90% purity), trioctylphosphine oxide (TOPO, 90% purity), selenium (Se), hexamethyldislthiane {$(TMS)_2S$}, 2 M of dimethylzinc {$Zn(CH_3)_2$} in toluene solution, anhydrous methanol, anhydrous toluene were purchased from Aldrich. TOP and TOPO were purified by vacuum distillation,[25,26] and kept in the glovebox. tris(tri-methylsilyl) arsenide {$(TMS)_3As$} was prepared as detailed in the literature.[32]

2. Synthesis of InAs Core Nanocrystals. Details of this synthesis are reported elsewhere,[26,27] and here we discuss a typical preparation: 3 g of TOP were heated in a three-neck flask on a Schlenk line under Ar atmosphere to a temperature of 300 °C with vigorous stirring. One milliliter of stock solution (see below), was rapidly injected, and the solution was cooled to 260 °C for further growth. The growth was monitored by taking the absorption spectra of aliquots extracted from the reaction solution. Additional injections were used to grow larger diameter cores. Upon reaching the desired size, the reaction mixture was allowed to cool to room temperature and was transferred into the glovebox. Anhydrous toluene was added to the reaction solution, and

(21) Daehne, S.; Resch-Genger, U.; Wolfbeis, O. S. Eds. *Near-Infrared dyes for high technology applications*; Kluwer Academic Publishers: Dordrecht, 1997.
(22) Murray, C. B.; Norris, D. J.; Bawendi, M. G. *J. Am. Chem. Soc.* **1993**, *115*, 8706.
(23) Micic, O. I.; Curtis, C. J.; Jones, K. M.; Sprague, J. R.; Nozik, A. J. *J. Phys. Chem.* **1994**, *98*, 4966.
(24) Nozik, A. J.; Micic, O. I. *MRS Bull.* **1998**, *23*, 24.
(25) Guzelian, A. A.; Katari, J. E. B.; Kadavanich, A. V.; Banin, U.; Hamad, K.; Juban, E.; Alivisatos, A. P.; Wolters, R. H.; Arnold, C. C.; Heath, J. R. *J. Phys. Chem.* **1996**, *100*, 7212.
(26) Guzelian, A. A.; Banin, U.; Kadanich, A. V.; Peng, X.; Alivisatos, A. P. *Appl. Phys. Lett.* **1996**, *69*, 1462.
(27) Peng, X.; Wickham, J.; Alivisatos, A. P. *J. Am. Chem. Soc.* **1998**, *120*, 5343.
(28) Banin, U.; Lee, J. C.; Guzelian, A. A.; Kadavanich, A. V.; Alivisatos A. P. *Superlattices Microstruct.* **1997**, *22*, 559.
(29) Allan, G.; Bastard, G.; Bocara, N.; Lanoo, M.; Voos, M. Eds. *Heterojunctions and Semiconductor Superlattices*; Springer: Berlin, Heidleberg, 1986.
(30) Wei, S.; Zunger, A. *Appl. Phys. Lett.* **1998**, *72*, 2011.
(31) Rogach, A.; Kershaw, S.; Burt, M.; Harrison, M.; Kornowski, A.; Eychmuller, A.; Weller, H. *Adv. Mater.* **1999**, *11*, 552.
(32) Becker, G.; Gutekunst, G.; Wessely, H. J. Z. *Anorg. Allg. Chem.* **1980**, *462*, 113.

the nanocrystals were precipitated by adding anhydrous methanol. The size distribution of the nanocrystals in a typical reaction was on the order of ±15%. This was improved using size selective precipitation with toluene and methanol as the solvent and nonsolvent, respectively.

Stock Solution of InAs Core. Under Ar atmosphere, 9 g of $InCl_3$ was dissolved in 30 mL of TOP at 260 °C with stirring. Then the solution was cooled, and taken into the glovebox. The stock solution was prepared by mixing a desired amount of $(TMS)_3As$ and $InCl_3$-TOP solution with the As:In molar ratios at 1:2 or 1:1.5.

3. Shell Growth. GaAs, InP, and CdSe Shells. TOP-capped InAs cores (5−20 mg) were dissolved in 3−6 g of TOP in a three-necked flask. Under Ar flow on a Schlenk line, the nanocrystal solution was heated to 260 °C, and the shell precursor solution of GaAs or InP, or CdSe (see below) was introduced into the hot solution by dropwise addition. The growth of core/shells was monitored by UV−vis spectroscopy of aliquots taken from the reaction flask. After growth to the desired shell thickness, the reaction mixture was cooled to room temperature. InAs/GaAs or InAs/InP, or InAs/CdSe core/shell nanocrystals passivated by TOP were obtained by precipitation using a mixture of methanol and toluene.

Stock Solution for Shells. GaAs Shell Precursor Solution. Three hundred mlligrams of $GaCl_3$ was dissolved in 10 mL of TOP by stirring in the glovebox. Then the stock solution was prepared by mixing $(TMS)_3As$ and $GaCl_3$ TOP solution with the As:Ga molar ratios at 1:4.

InP Shell Precursor Solution. Concentrated $InCl_3$ TOP solution for InAS core growth was diluted 10 times with TOP. Then this diluted $InCl_3$ TOP solution was mixed with $(TMS)_3P$ at P:In molar ratios of 1:1.2−1.5.

CdSe Shell Precursor Solution. Selenium (80 mg) was dissolved in 7 mL of TOP in the glovebox. Then $Cd(CH_3)_2$ was added to this TOPSe solution with Se:Cd molar ratios at 1:1.2.

ZnS and ZnSe Shells. InAs nanocrystals (5−20 mg) capped with TOP, were dissolved in a mixture of TOP and TOPO (2 g of TOP and 2 g of TOPO) at 60 °C under Ar. The nanocrystal solution was heated to 260 °C, and the stock solution of ZnS or ZnSe shells was introduced by dropwise addition. The reaction was stopped when the demanded shell thickness was reached. Toluene was added to the solution, and the nanocrystals were precipitated by methanol and separated from the growth solution.

Stock Solution for Shells. ZnSe shell stock solution was prepared by mixing a TOPSe solution (1.2 mg/mL Se in TOP) and equimolar amounts of 2 M $Zn(CH_3)_2$ toluene solution. ZnS shell stock solution was obtained by mixing $(TMS)_2S$−TOP solution (1.8 mg/mL $(TMS)_2S$ in TOP) and 2 M of $Zn(CH_3)_2$ toluene solution with molar ratio: 1:1.

B. Characterization. UV−vis−NIR absorption spectra were measured using a Shimadzu UV1601 or UV 3101pc spectrophotometer. Nanocrystals were dissolved in toluene for the measurement.

Photoluminescence and Fluorescence QY determination. Photoluminescence (PL) experiments were performed using a He−Ne laser (632 nm, output power: 3 mW, spot size: 3 mm) or a monochromatized arc Xenon lamp (150 W) as the excitation source. The excitation beam was chopped at 270 Hz. The emission was collected at a right angle configuration, dispersed by a monochromator and detected by a liquid nitrogen cooled InGaAs diode or a InGaAs PIN photodetector with lock-in amplification. The fluorescence spectra were corrected for the response of the detection system, using a correction curve determined by measuring the spectrum of a standard tungsten−halogen lamp.

Room-temperature fluorescence quantum yields (QYs) of the nanocrystal solutions were determined by comparing the emission with the integrated emission of the laser dye IR 125 in DMSO (dimethyl sulfoxide) with equal optical densities at the excitation wavelength. The QY for the IR 125 laser dye was reported to be 0.13 in DMSO.[33] In a typical experiment, we measured the fluorescence of a solution of core InAs nanocrystals in toluene and in the same conditions measured the fluorescence of the dye solution using 764 nm excitation from the monochromatized Xe lamp, which is close to the peak of the dye absorption. Both solutions had an equal optical density at 764 nm, of ~0.3. Comparing the integrated fluorescence intensity, corrected for the detection system response, of these two solutions, provided us with the QY of the core InAs nanocrystals. The refractive index of the two solvents toluene and DMSO, are nearly identical (1.49 versus 1.48 respectively[34]), and therefore the quadratic refractive index correction which amounts to a factor of only 1.02 was not needed.[35] Then, for the core/shells in toluene, we used the excitation wavelength of 632 nm of the He−Ne laser, which provided improved S/N. We measured the emission of the core/shell solution and of InAs solution with equal optical density (~0.3) at 632 nm, and compared the corrected integrated intensity of the fluorescence of these solutions, allowing us to extract the QY for core/shells.

X-ray Photoelectron Spectroscopy (XPS). XPS measurements were performed on a Perkin-Elmer PHI 5600 ESCA system. Data were obtained with Al Kα radiation (1486.6 eV) at 200 W. Survey spectra were collected in the range of 0~1400 eV with a 187.85 eV pass energy detection. High-resolution spectra for the quantitative calculations were obtained at a 11.75 eV pass energy with a resolution of 0.025 eV per step interval. Typical high-resolution scans were collected for 10−30 min per element. Measurements were performed at pressures lower than 1×10^{-8} Torr. Spectra were calibrated using the position of the Au 4f peaks present in all spectra as a standard. These measurements were performed on nanocrystal films of monolayer thickness, linked by hexane dithiols to a Au coated substrate.[36]

X-ray Diffration (XRD). Powder X-ray diffraction patterns were measured on a Philips PW 1830/40 X-ray diffractometer with Cu Kα radiation. Approximately 10 mg of nanocrystals were dispersed in minimum volume of toluene. The nanocrystal solution was deposited onto low-scattering quartz plates, and the solvent was evaporated under mild vacuum.

Transmission Electron Microscopy (TEM). High-resolution TEM (HRTEM) images were obtained using a JEOL-JEM 2010 electron microscope operated at 200 kV. Low-resolution TEM images were obtained using a Philips CM 120 microscope operated at 120 kV. Samples for TEM were prepared by depositing a drop of a nanocrystal solution in toluene onto a copper grid supporting a thin film of amorphous carbon. The excess liquid was wicked away with filter paper, and the grid was dried in air.

Shell thickness is reported in monolayers (ML), with 1 ML equal to the d_{111} lattice spacing of the shell material (e.g., $d_{111} = 3.498$ Å for InAs). The shell thickness was determined by measuring the sizes of nanocrystals from low resolution TEM images of core and core/shell nanocrystals grown on these cores. We subtracted the average radius of the cores, from the average radius of core/shells as determined from these measurements. Sizes of nanocrystals measured by low resolution TEM images are systematically larger than those measured by HRTEM images as is known from other studies.[37] This is due to the insensitivity of the HRTEM to a possibly disordered surface layer but the relative measurement with the low resolution TEM that we employed for shell thickness determination avoids this error. For several samples, we also determined the shell thickness from HRTEM, and the shell thickness were consistent with those from the low-resolution TEM. The radius of the core nanocrystals reported in this study was obtained from a sizing curve measured from HRTEM of InAs nanocrystals as determined previously.[37]

Results and Discussion

1. Synthesis of Core/Shell Nanocrystals. The preparation of the InAs core/shell nanocrystals is carried out in a two-step process. In the first step the InAs cores are prepared using the injection method with TOP as solvent, which allowed us to obtain hundreds of mg of nanocrystals per synthesis.[27] We used size-selective precipitation to improve the size distribution of cores to $\sigma \approx 10\%$. In the second step, the shells of the various

(33) Reference 21, pp 149.

(34) Riddick, J.A; Bunger, W. B. *Organic Solvents*; Wiley: New York, 1970.

(35) Demas, J. N.; Crosby, G. A. *J. Phys. Chem.* **1971**, *75*, 991.

(36) Katari, J. E. B.; Colvin, V. L.; Ailivisatos, A. P. *J. Phys. Chem.* **1994**, *98*, 4109.

(37) Banin, U.; Lee, C. J.; Guzelian, A. A.; Kadavanich, A. V.; Alivisatos, A. P.; Jaskolski, W.; Bryant, G. W.; Efros, A. L.; Rosen, M. *J. Chem. Phys.* **1998**, *109*, 2306.

materials were grown on these cores. This two step approach follows the methods developed for synthesis of the II−VI core/shell nanocrystals.[14,16]

Initially we attempted to carry out the growth of III−V semiconductor shells, InP and GaAs, at a temperature of 160 °C in TOP. Low temperature reduces the rate of nucleation of nanocrystals of the shell material, which is an undesired process competing with shell growth. In addition, the alloying process of core and shell materials is less likely at low temperatures. However, growth could not be achieved at this low temperature. Only for higher temperatures, $T > 240$ °C, these shells could be grown. This minimal temperature is needed to overcome the reaction barrier for the precursors. Above this limit we achieved controlled growth of InP shells of varying thickness on cores with different sizes.

Thin GaAs shells could also be grown, but unlike InP shells, growth was limited to a thickness of <2 ML. This difference may be related to strong bonding of Ga to TOP, consistent with the observation that it is difficult to synthesize GaAs nanocrystals in this way.[38] An additional difference between the GaAs and the InP shells is in the solubility of the core/shell nanocrystals of each kind. InAs/InP core/shells, are readily soluble in organic solvents, after precipitation of the nanocrystals from the growth solution. Special conditions were required to obtain good solubility of the InAs/GaAs core/shells. We used an increased ratio of Ga:As (4:1) in the precursor solution, and annealed the InAs/GaAs nanocrystals in the growth solution for several hours, at a temperature of 260 °C.

In contrast to the III−V semiconductor shells, the growth of the II−VI semiconductor shells, CdSe, ZnSe, and ZnS, was observed already at low temperatures above 150 °C. For CdSe shells, following the prototypical CdSe nanocrystal synthesis,[22,36] we first tried to use TOPO as the growth medium. In this case, substantial nucleation of CdSe nanocrystals was observed as detected by the appearance of a characteristic peak in the absorption spectrum. This nucleation could not be avoided even with very dilute precursor solution and slow precursor addition. To limit the nucleation and achieve controlled shell growth, we found that TOP could be used instead of TOPO. This is consistent with stronger bonding of Cd to TOP versus TOPO. Another approach to limit nucleation of nanocrystals of the shell material was previously used successfully in the synthesis of CdSe/CdS core/shells, where the S-to-Cd ratio was increased to 2.1:1.[15] We attempted to reduce the nucleation of CdSe by increasing the ratio of Se:Cd in the precursor solution, but the solubility of the final nanocrystals was poor.

InAs/ZnSe and InAs/ZnS core/shells, were initially grown in TOP, but their solubility after separation from the growth solution was poor as the TOP ligands were easily removed by methanol. Additionally, upon growth of thick ZnS shells, substantial nucleation of ZnS nanocrystals was observed by XRD measurements. To overcome these difficulties, we used instead of TOP, a mixture of TOP−TOPO as the growth solution. In this case nucleation could be minimized, and soluble nanocrystals were obtained. The growth rate of ZnSe and ZnS shells was substantially slower for the TOP−TOPO mixture compared with that for TOP. These features are consistent with stronger bonding of Zn to TOPO versus TOP, as was reported in the synthesis of ZnSe nanocrystals.[39] Cd is a softer Lewis acid than Zn, and binds stronger to TOP, a softer Lewis base than TOPO, while Zn, the harder Lewis acid, binds more strongly to TOPO the harder Lewis base. This follows the general hard−soft concept for interaction strength between Lewis acids and bases.[40]

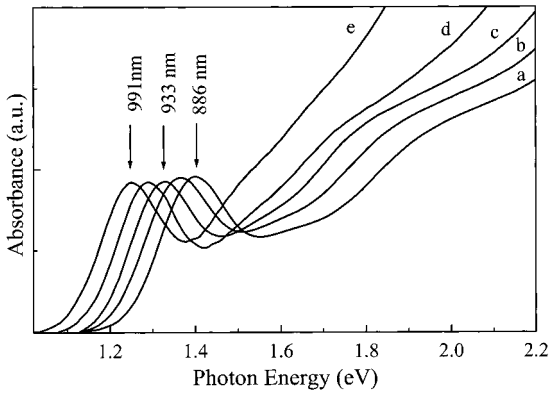

Figure 2. Evolution of the absorption spectra during the growth of InP shells on InAs cores with an initial radius of 1.3 nm (a). The InP shell thickness in number of monolayers (ML) is: (b) 0.5, (c) 1.1, (d) 1.7, (e) 2.5.

2. Optical Characterization. The most direct and immediate probes for shell growth are the absorption and fluorescence spectra. Figure 2 shows the sequence of absorption spectra measured for aliquots taken from the reaction solution during the growth of InP shells on InAs cores with an initial radius of 1.3 nm. The first absorption peak shifts to the red as we reported earlier for growth of an InP shell on a bigger core.[18] The red-shift occurs because the conduction band offset between InAs and InP is smaller than the confinement energy of the electron, and as the shell grows, the electron wave function extends to a larger box, and its confinement energy is lowered. As the electron effective mass, m_e^*, in InAs is extremely small ($m_e^* = 0.024m_e$, m_e is the mass of the free electron[41]), it is highly delocalized, and a large potential step is required to confine it to the core. The observed red-shift also rules out the formation of an alloy of the core and shell materials.[15] In the case of an alloy, the band gap should be intermediate between the band gaps of nanocrystals of the composing materials, InP and InAs, of the same size. The band gap of bulk and of nanocrystalline InP is substantially larger compared with the band gap of InAs, and thus a blue-shift is expected for the alloy nanocrystal. The spectral features remain sharp during the reaction, indicating that the growth is controlled and that the size distribution is maintained. However, the fluorescence of the InAs/InP core/shells is quenched substantially as compared to the original cores.

For CdSe, which has a conduction band offset similar to that of InP, shell growth also leads to a red-shift of the absorption onset. Figure 3A−B shows the evolution of the absorption and the emission spectra during growth of InAs/CdSe core/shells with two different initial core radii, 1.2 nm (Figure 3A), and 2.5 nm (Figure 3B). As in the case of InP shells, this red-shift results from the lower confinement energy of the electron whose wave function extends to the shell region. In this case the sharpness of the spectral features is partially washed out during the growth. In contrast to InAs/InP core/shells, the band gap fluorescence QY for InAs/CdSe core/shells is substantially enhanced, up to a maximum value of 21%, nearly 20 times larger than the QY of the cores. Typical values of QY from

(38) Guzelian, A. A. Synthesis and Charaterization of III−V Semiconductor Nanocrystals. Ph.D. Thesis, University of California, Berkeley, 1996.

(39) Hines, M. A.; Guyot-Sionnest, P. *J Phys. Chem. B* **1998**, *102*, 3655.

(40) Lagowski, J. J. *Modern Inorganic Chemistry*; Marcel Dekker: New York, 1973; pp 320−322.

(41) Madelung, O.; Schulz, M.; Heiss, H. Ed, *Landolt-Bornstein: Numerical Data and Functional Relationships in Science and Technology*, New Series, Vol. 17; Springer-Verlag: New York, 1982.

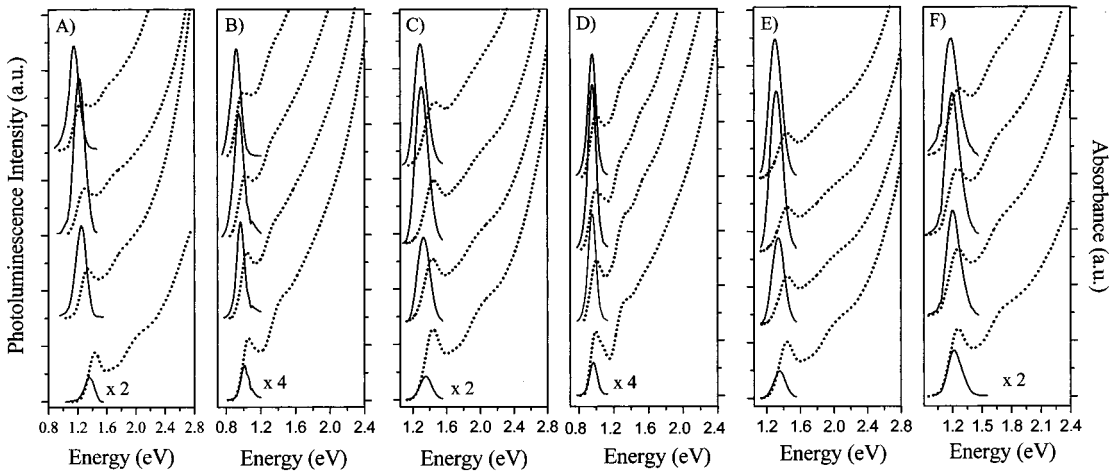

Figure 3. Evolution of absorption (dotted lines), and photoluminescence (solid lines) for growth of core/shells. The PL spectra are given on a relative scale for comparison of the enhancement of QY with shell growth. (A) InAs/CdSe with initial core radius of 1.2 nm. The shell thickness (in number of ML) and QY for the traces from bottom to top are respectively: 0, 1.2%; 0.6, 13%; 1.2, 21%; 1.8, 18%. (B) InAs/CdSe with initial core radius of 2.5 nm. The shell thickness (in number of ML) and QY for the traces from bottom to top are respectively: 0, 0.9%; 0.7, 11%; 1.2, 17%; 1.6, 14%. (C) InAs/ZnSe with initial core radius of 1.2 nm. The shell thickness (in number of ML) and QY for the traces from bottom to top are respectively: 0, 1.2%; 0.6, 9%; 1.5, 18%; 2.5, 14%. (D) InAs/ZnSe with initial core radius of 2.8 nm. The shell thickness (in number of ML) and QY for the traces from bottom to top are respectively: 0, 0.9%; 0.7, 13%; 1.3, 20%; 2.2, 15%. (E) Inas/ZnS with initial core radius of 1.2 nm. The shell thickness (in number of ML) and QY for the traces from bottom to top are respectively: 0, 1.2%; 0.7, 4%; 1.3, 8%; 1.8, 7%. (F) InAs/ZnS with initial core radius of 1.7 nm. The shell thickness (in number of ML) and QY for the traces from bottom to top are respectively: 0, 1.1%; 0.6, 5%; 1.3, 7.1%; 2.2, 6.3%.

InAs/CdSe core/shells range between 18 and 21%. These values of the QY compete favorably with QY values for organic NIR laser dyes.[21] We assign this pronounced difference in emission of InP versus CdSe shells to the different quality of the outer surface of the nanocrystals. In both cases, the similar and relatively small conduction band offset leads to a substantial probability of presence for the electron wave function at the nanocrystal surface. As a result, for both cases the emission is still sensitive to the outer surface, and susceptible to trapping in un-passivated surface sites. Indeed, this problem is known for InP nanocrystals prepared in TOP/TOPO, which have very low fluorescence QY that could be enhanced by surface treatments such as oxidation and etching.[25,42] CdSe−TOP/TOPO coated nanocrystals on the other hand, display band gap emission with room-temperature QY of a few percent.[43]

Much larger band offsets for ZnSe and ZnS relative to InAs, provide strong motivation to grow shells of these materials on InAs. The evolution of the absorption and emission spectra for ZnSe and ZnS shell growth on cores with various radii, is presented in Figure 3C,D and 3E,F, respectively. For both core/shells, the absorption onset is nearly the same as in the original core. This can be explained by the large conduction and valence band offsets of ZnSe and ZnS relative to InAs, which create a substantial potential barrier for the electron and hole wave functions at the core/shell interface. Unlike the CdSe and InP shells, here the electron and hole wavefucntions are both confined primarily to the core region, and thus the band gap does not shift from the value of the core. As shown in Figure 3C−F, the fluorescence QY is enhanced for both shells. For ZnSe the maximum QY values are 20% (typical maximal QY values achieved in other reactions was 18−21%), while in ZnS the maximum QY is 8% achieved for a shell thickness of 1.2−1.8 ML. With further shell growth, the QY decreases. This reduction may be assigned to trapping of the charge carriers at the core/shell interface. The lattice mismatch between InAs and both ZnSe and ZnS is large. In thin shells the strain can still be sustained and epitaxial growth of the shell on the core can occur. With further shell growth, defects may form at the core/shell interface, and they could trap the carriers, leading to the gradual reduction of QY in the thicker shells. A similar observation was reported for the II−VI semiconductor core/shells CdSe/ZnS, and CdSe/CdS.[15,16]

In CdSe shells (Figure 3A,B), the QY increases, up to the maximum value which occurs for relatively thin shells (1−1.5 ML). Further growth also leads to some reduction of the QY. The lattice mismatch between InAs and CdSe is zero, but CdSe nanocrystals grown in these conditions favor the wurtzite structure over the cubic one, which is inherent for InAs. This may lead to formation of defects, which could trap the carriers in thicker CdSe shells.

The newly developed InAs/ZnSe and InAs/ZnS core/shells extend the control afforded for the electronic properties of the composite nanocrystals. As an example for the flexible control we synthesized two types of core/shells, InAs/ZnSe and InAs/CdSe, which emit strongly at 1.3 μm, a wavelength with significant technological importance in fiber-optic communications. Figure 3B presents the absorption and emission for a CdSe shell overgrown on a core with a radius of 2.5 nm. The core band gap emission is at 1220 nm, and with the growth of the shell the emission shifts to the red. This is accompanied by substantial enhancement of the QY, up to a value of 17% achieved at 1306 nm. For ZnSe shells the band gap hardly shifts. Figure 3D shows that using a bigger core, with radius of 2.8 nm, we could achieve a high QY of 20% at 1298 nm by growing the ZnSe shell.

3. Chemical and Structural Characterization. X-ray Photoelectron Spectroscopy (XPS). We used XPS to examine the chemical composition of our core/shells.[36,44] Figure 4 shows the XPS survey spectra for InAs cores, 1.7 nm in radius and for InAs/CdSe core/shells prepared with the same core and with

(42) Micic, O. L.; Cheong, H. M.; Fu, H.; Zunger, A.; Sprague, J. R., Mascarenhas, A.; Nojik, A. J. *J. Phys. Chem. B* **1997**, *101*, 4904.

(43) Norris, D. J.; Sacra, A.; Murry, C. B.; Bawendi, M. G. *Phys. Rev. Lett.* **1994**, *101*, 8455.

(44) Hoener, C. F.; Allan K. A.; Bard, A. J.; Campion, A.; Fox, M. A.; Mallouk, T. E.; Webber, S. E.; White, J. M. *J. Phys. Chem.* **1992**, *96*, 3812.

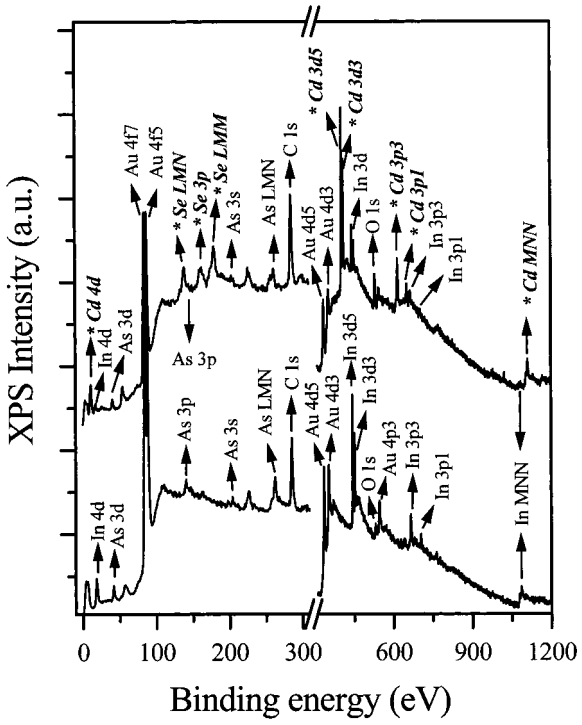

Figure 4. XPS survey spectrum for InAs cores with radius of 1.7 nm (lower trace), and for InAs/CdSe core/shells with shell thickness of 3 ML (top trace). The assignment of the peaks is indicated. The new peaks in the XPS spectrum for the core/shells associated with Cd and Se are marked by star and emphasized in bold italic type.

shell thickness of 3 ML. Indium and arsenic peaks are clearly resolved for the core (lower spectrum). Additional peaks belonging to Cd and Se, the shell materials, can be identified in the core/shells (top spectrum). The ratio of the XPS peak heights between core and core/shell for the core atoms, is energy-dependent. The relative intensity of the peaks at high binding energies (e.g., In_{MNN}), which have a small kinetic energy and thus a small escape depth, is quenched more upon shell growth, compared with the peaks at small binding energy and large escape depth (e.g., As_{LMN}).

High-resolution XPS provides quantitative evidence for shell growth based on the finite escape depth, λ, of photoelectrons from the core atoms.[16] The typical escape depths are on the order of the shell thickness and the photoelectron signal from core atoms should decrease accordingly in the core/shell structure. The XPS signal intensity, I, at depth z is given by[36]

$$I = nfoyF(KE)\int_V e^{-z/\lambda(KE)}\,dv \qquad (1)$$

where n is the density of atoms, f is the X-ray flux, σ is the cross section of the photoelectronic process, y is the photoelectron emission quantum yield, $F(KE)$ is the instrument response function which depends on the energy KE. For a flat geometry, the value of the integral in eq 1 is λ − the photoelectron escape depth, and then eq 1 can be simplified to $I = nS$, where S is the atom and kinetic energy-dependent sensitivity factor. For the nanocrystals, where the radius r is on the order of λ, the assumption of flat geometry has to be corrected by carrying out the integration in eq 1 over the nanocrystal volume. For this integration we assume a spherical shape for the nanocrystals.[36,44]

The application of XPS to study shell growth is demonstrated in Figure 5. Figure 5a shows the XPS data for InAs/ZnSe core/shells with initial core radius of 1.7 nm. We performed high-resolution XPS measurements on a sequence of core/shell samples with varying thickness. The figure shows the experimental results (squares) for the log of the ratio of the In_{3d5} to the In_{MNN} Auger peak, normalized by the ratio in the core. The ratio increases upon ZnSe shell growth.[16] The number of atoms, n, for the two peaks is identical and the increase of the ratios is due to the difference in the escape depths, which is lower for the Auger peak. As a result, the shell growth leads to larger reduction in the relative intensity of the Auger peak. To check these effects we simulated the expected ratio for a spherical geometry assuming a core/shell configuration (solid line), or alloy formation (dashed line). Clearly, only the calculated ratio for the core/shell structure is in agreement with experimental data. The following photoelectron escape depths (λ) under Al Kα radiation (1486.6 eV), were used in the simulations in the InAs core region: $In_{3d5/2}$ 19.2 Å; In_{MNN} 12.2 Å. The values in the ZnSe shell region were 16 and 11.6 Å respectively.[45,46]

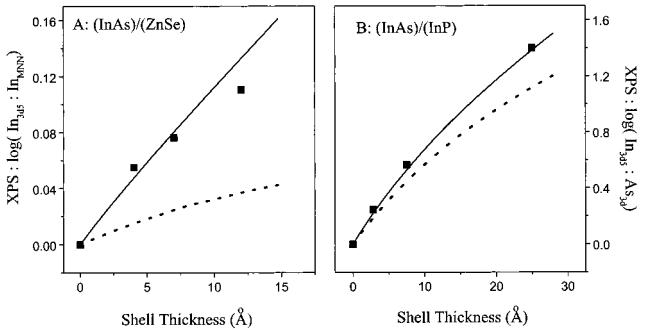

Figure 5. Summary of high-resolution XPS data for InAs/ZnSe and InAs/InP core/shells. (A) For InAs/ZnSe core/shells, the log of the ratio of the intensities of the In_{3d5} to the In_{MNN} is shown, versus the shell thickness. (B) For InAs/InP core/shells, the log of the ratio of intensities of the In_{3d5} to As_{3d} is shown, versus the shell thickness. In both cases the ratio is normalized to the ratio in the cores. Squares: experimental data. Solid line: calculated ratio for core/shell structure. Dashed line: calculated ratio for alloy formation. See text for details.

We also checked by simulation, the sensitivity of the XPS ratio to non-centered spherical core/shell particles. In this case the position of the center of the core within the core/shell nanocrystals was changed from the middle up to a position in which the core and core/shell surfaces were tangent. Such a situation is relevant for the case of a non-homogeneous (although still spherical) shell growth around the core. We averaged the correction factor over a distribution of different orientations of such non-centered core/shells, which are present on the substrate. Only small changes were detected in the XPS ratio in this case compared with the case of a centered core/shell. For thin shells the difference is negligible, and even for thick shells (3 ML), the change is small, on the order of ~5%. Therefore, the XPS ratio cannot be used to distinguish between this case and centered core/shells.

Figure 5b shows the XPS data for InAs/InP core/shells. The figure shows the experimental results (squares) for the log of the ratio of the In_{3d5} peak to the As_{3d} peak normalized to the ratio in the core. The ratio increases upon shell growth, first and foremost due to the addition of In atoms in the shell region. Further increase of the ratio should result from the reduction in the relative arsenic signal due to the finite escape probability of the photoelectrons through the shell region. The simulation of the ratio assuming a core/shell configuration (solid line) fits

(45) Tanuma, S.; Powell, C. J.; Penn, D. R. *Surf. Interface Anal.* **1991**, *17*, 927.

(46) Somorjai, G. A. *Chemistry in Two Dimensions: Surfaces*; Cornell University Press: Cornell, 1981.

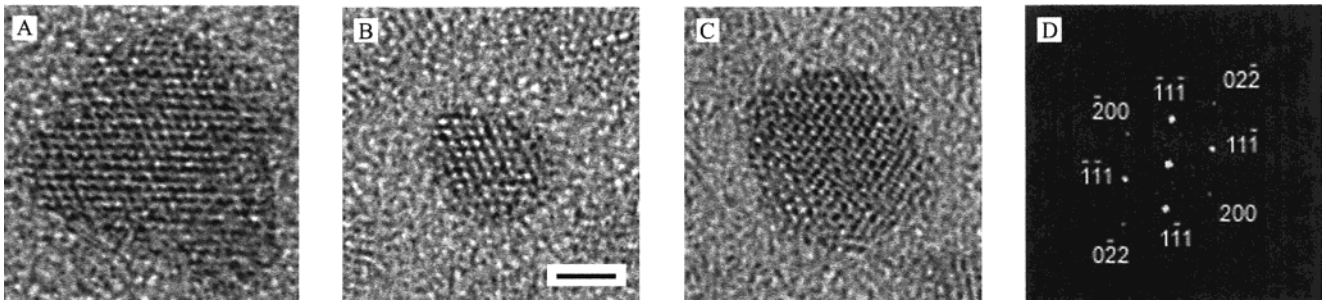

Figure 6. HRTEM images of InAs/InP core/shell (frame A, core radius 1.7 nm, shell thickness 2.5 nm), InAs core (frame B, core radius 1.7 nm), and InAs/CdSe core/shell (frame C, core radius 1.7 nm, shell thickness 1.5 nm). The scale bar is 2 nm. The nanocrystals are viewed along the [011] zone axis. Frame D shows the Fourier transform of image C, and the pattern corresponds to the diffraction pattern from the 011 zone of the cubic crystal structure.

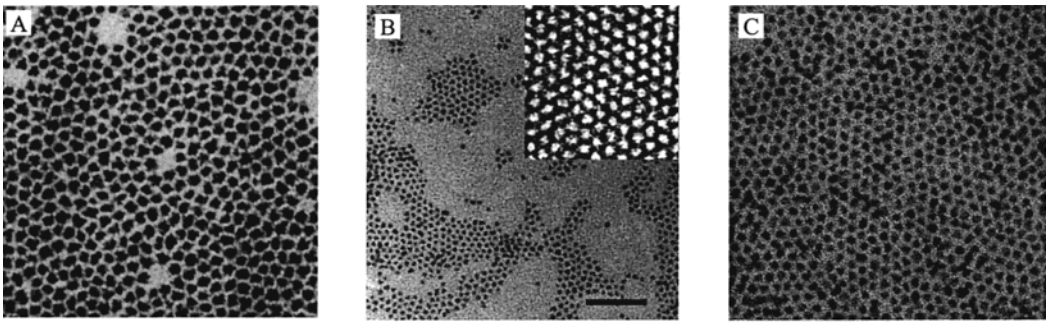

Figure 7. TEM images of InAs/InP core/shells (frame A, core radius 1.7 nm, shell thickness 2.5 nm), InAs cores (frame B, core radius 1.7 nm), and InAs/CdSe core/shells (frame C, core radius 1.7 nm, shell thickness 1 nm). The scale bar is 50 nm. The inset of frame B (70 × 70 nm), displays a portion of a superlattice structure formed from the InAs cores.

the experimental results. The simulated curve for alloy formation (dashed line), predicts a lower ratio although it also increases with shell growth because of the addition of In atoms. The following photoelectron escape depths (λ) were used in the calculations in the InAs core region: As_{3d} 24.8 Å, $In_{3d5/2}$ 19.2 Å. The respective values in the InP shell were 24 and 18.6 Å.[45]

Transmission Electron Microscopy. Figure 6 presents HRTEM images of core and core/shell nanocrystals. Frame B shows a micrograph of an InAs core with radius of 1.7 nm, and frames A and C respectively show InAs/InP and InAs/CdSe core/shell nanocrystals with thick shells grown on similar cores. The crystalline interior is viewed along the [011] zone axis of the cubic lattice. The cubic lattice is resolved for the InAs/CdSe core/shell as well, as clearly revealed also by the Fourier transform of the image presented in Figure 6D. CdSe nanocrystals grown in such conditions form the wurtzite structure, but here they adopt the cubic structure on the InAs core. For all three cases, the fringes are visible across the entire nanocrystals in accordance with epitaxial shell growth in these particles.

Figure 7 shows TEM images for close packed nanocrystal monolayers of InAs cores with radius 1.7 nm (B), InAs/InP core/shells with shell thickness of 2.5 nm (A), and InAs/CdSe coreshells (C) with shell thickness of 1 nm grown on similar cores. Furthermore, InAs core nanocrystals can form superlattices (SL), as seen in the inset of frame B. The superlattice is prepared by slow solvent evaporation, and its formation further indicates that the size distribution of the InAs cores is narrow.[47] The width of the size distribution of cores was estimated from the TEM measurements to be ~8% (σ), for core/shells the distribution after growth of thick shells broadens to ~12%.

The shell thickness determined from TEM was also used to estimate the yield of shell growth. This yield is material dependent. For CdSe and InP shells, the growth yield is larger than 90%. For thin ZnSe and ZnS shells, the growth yield ranges from 60 to 80% depending on the TOP/TOPO ratio. Higher growth yields are obtained for larger TOP fractions. The growth yield in thick ZnSe and ZnS shells (over 3 ML), increases to over 90%.

X-ray Diffraction. Powder XRD patterns for the InAs core, 1.7 nm in radius, and for InAs/InP core/shells with increasing thickness is presented in Figure 8. The InAs XRD pattern consists of the characteristic peaks of cubic InAs, which are broadened because of the finite crystalline domain size.[26] With InP shell growth, the diffraction peaks shift to larger angles consistent with the smaller lattice constant for InP compared with InAs. The shift is most clearly resolved for the high angle peaks. In addition, the diffraction peaks narrow. We demonstrate this for the (111) peak shown in the inset of Figure 8. This narrowing indicates that the crystalline domain is larger for the core/shells providing direct evidence for epitaxial growth mode of the shell.[18] The relatively simple diffraction pattern for cubic InAs allows for a clear observation of the narrowing as the shell is grown. In contrast, in the case of cores/shells with CdSe cores, the narrowing is masked by the complex diffraction pattern of the wurtzite structure.[15,16]

The XRD patterns for a series of core/shells with different shell materials and varying thickness are displayed in Figure 9 (filled circles). The general pattern of the cubic lattice is maintained for all materials. The diffraction peaks narrow with shell growth in the case of CdSe, ZnSe, and GaAs shells for the reasons discussed above. But this is not the case for ZnS, probably due to the very large lattice mismatch of ZnS and InAs (10.7%). In this case, the large strain may lead to cracking at the InAs/ZnS interface already at early growth stages. Moreover, ZnS nanocrystals in these growth conditions preferentially form the wurtzite structure, which may create additional defects upon

(47) Murray, C. B.; Kagan, C. R.; Bawendi, M. G. *Science* **1995**, *270*, 1335.

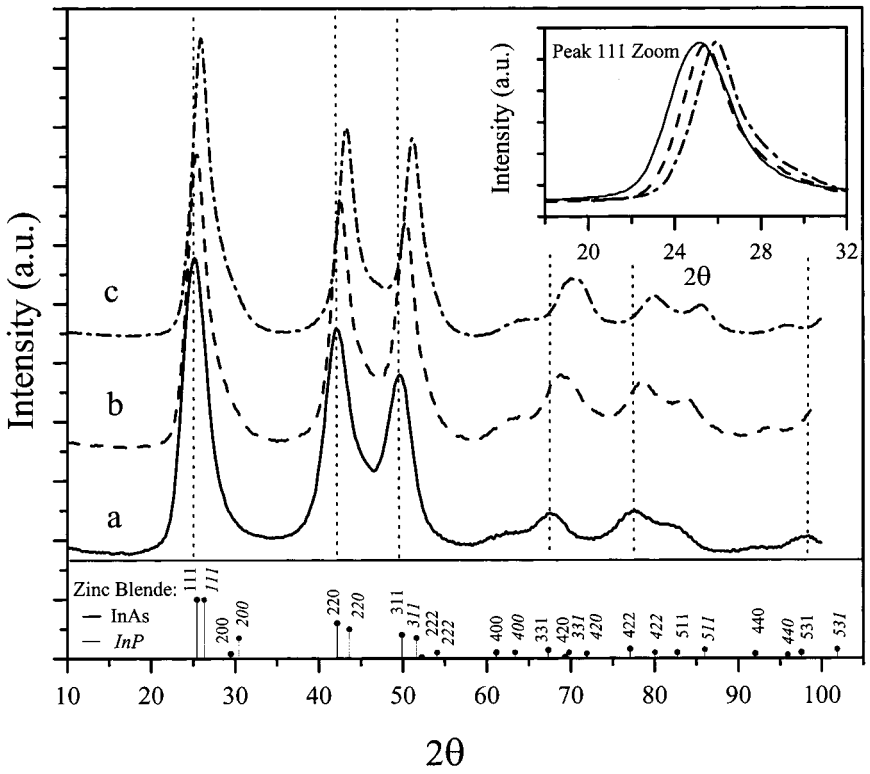

Figure 8. XRD patterns for InAs cores with radius of 1.7 nm (trace A, solid line), and InAs/InP core/shells with shell thickness of 2.4 ML (B, dashed line), and 6.2 ML (C, dot−dashed line). The inset shows a zoom of the 111 peak. The diffraction peak positions of bulk cubic InAs (dark) and *InP* (light, italic) are indicated.

shell growth. Both effects may explain the relatively small enhancement of the PL QY for the ZnS shells.

To further prove our interpretation of the XRD data and to obtain more quantitative information about the core/shell structures, we simulated the powder diffraction patterns. The method of calculation follows that published earlier.[16,22,48] We built nanocrystals by stacking planes along the (111) axis of the cubic lattice. The sum of the specified core radius, r_c, and shell thickness, r_s, was used to carve out the nanocrystal assuming a spherical shape. We also added the possibility of surface disorder, as well as the temperature effect.

The experimental data (filled circles), and the simulation results (thin lines) for the core and a series of core/shells are displayed in Figure 9. The simulation of the cores fits the experimental data very well. The fit was obtained using the simulated XRD pattern for an equally weighted combination of two kinds of core nanocrystal structures with the same radii, differing in the (111) plane stacking sequence as detailed in Table 1.[49] Both nanocrystal structures have three stacking faults. The experimental diffraction intensity between the (220) and the (311) peaks does not go to zero, while in the simulated pattern for nanocrystals without stacking faults the value is close to zero. Thus, three stacking faults along the (111) direction are required to quantitatively reproduce the experimental pattern. Introduction of surface disorder has little effect on the simulated patterns. We also varied the shape of the core and for cube, tetrahedron and spherical shapes the patterns are nearly similar. The same combination of core structures was used in all of the simulations of the XRD patterns for the core/shell structures. The relevant parameters for the structures used in the simulation are given in Table 1.

For InAs/CdSe core/shells, the lattice mismatch is zero. The experimental peak positions do not shift with shell growth. This is well-reproduced in the simulation. An additional stacking fault was added in the shell region for the thicker shell of 3 ML, to better reproduce the experimental pattern.

For the other core/shells there is a lattice mismatch, which ranges from 3.13% for InP, to 10.7% for ZnS. A gradual shift of the diffraction peaks with shell growth toward larger angles, is observed for these core/shells (Figure 9). This means that the lattice spacing is modified in the shell region. To achieve epitaxial growth mode, atoms in both core and shell regions at the core/shell interface must have identical lattice spacings. To simulate the smooth switching of the lattice spacing from the core to the shell, we used a Fermi-like switching function

$$a(r) = a_s + \frac{a_c - a_s}{e^{(r-r_c)/T} + 1} \qquad (2)$$

here *a(r)* is the lattice constant at radius r, a_c, and a_s are the lattice spacings for the bulk core and shell materials respectively, r_c is the radius of the core, and T is the switching length factor. This switching provides a physical model for understanding the epitaxial growth mode, while reproducing the observed change in the peak positions upon shell growth. We studied the effect of switching on the diffraction patterns of core/shells, by varying T from nearly 0 to 9 Å. We found that the diffraction pattern is only slightly sensitive to the magnitude of T. This may be due to the inherent symmetry of the Fermi-like switching function, eq 2, in the core and shell regions. Over the switching range, the lattice constant changes to smaller values for the core relative to pure InAs, and increases in the shell relative to the respective pure materials. The X-ray scattering factor for InAs is larger than that of all shell materials,[50] and the overall effect is that the peak positions shift slightly to high angles with increasing

(48) Wickham, J. N.; Herhold, A. B. Alivisatos, A. P. *Phys. Rev. Lett.* **2000**, *84*, 923.

(49) Wickham, J. N.; Alivisatos, A. P. Private communication.

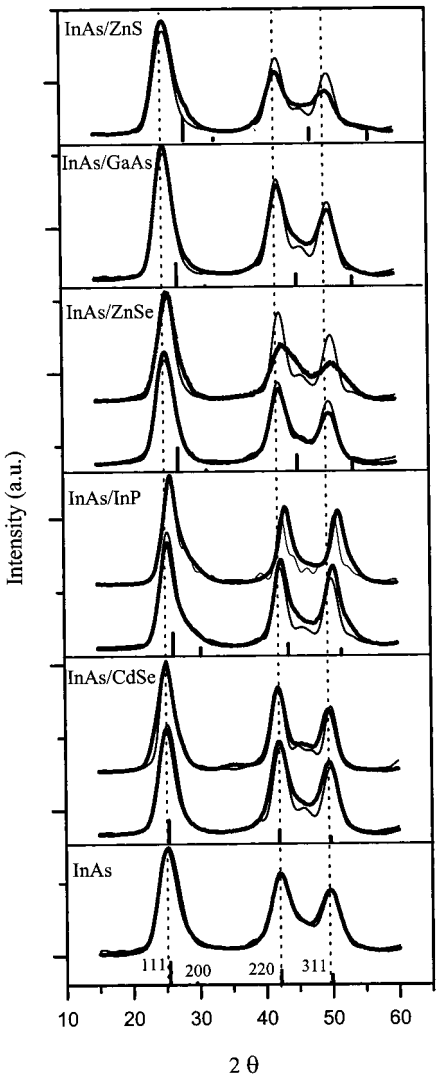

Figure 9. X-ray diffraction patterns for InAs cores and various core shells. The experimental curves (filled circles), are compared with the simulated curves (thin solid lines). See text and Table 1 for the details of the simulated structures. The markers on the bottom of each frame indicate the bulk diffraction peak positions and the relative intensities for the InAs core material (lower frame), and the various shell materials (other traces). The vertical dashed lines indicate the positions of the InAs core nanocrystal diffraction peaks.

Table 1. Parameters Used in the XRD Simulations

	radius or shell thickness (Å)	number of atoms	number of stacking faults	planes per stacking fault
core (a)[a]	34	751	3	3.7
core (b)[a]	34	729	3	3.7
CdSe shell	3.5	∼1500	3	4.5
	11	∼3400	4	4.3
InP shell	8	∼2400	3	5.2
	21	∼8300	6.5	3.6
ZnSe shell	3.6	∼1300	3	4.4
	8	∼2400	3	5.3
GaAs shell	4.5	∼1500	3	4.6
ZnS	4.5	∼1500	3	4.6

[a] The stacking sequence for the two cores, along the (111) direction, are a: 12312121321 and b: 12321312321.

T. In our simulations we set *T*, the switching length factor, to 6 Å corresponding to a shell thickness of ∼2 ML.

The simulated patterns reproduce the two main effects observed upon shell growth in InAs/InP, InAs/ZnSe, and InAs/GaAs core/shells, namely the shifting of all the diffraction peaks to larger angles, and the narrowing of the peaks (Figure 9). This provides further evidence for the epitaxial shell growth mode. For InAs/ZnS, no narrowing was observed in the experimental diffraction pattern indicating that here, the interface region is not fully epitaxial as explained above. Similar to the case of InAs/CdSe core/shells, for the thick InP shells (6.2 ML), stacking faults had to be added in the shell region to better reproduce the experimental pattern. On average, we find that a stacking fault exists for every four to five layers in InAs core/shell nanocrystals (Table 1). In these stacking faults the bonds of atoms remain fully saturated and charge carrier traps do not necessarily form. Therefore, it is likely that these planar stacking faults do not reduce the fluorescence QY substantially.

Large deviations are observed for InAs/ZnSe with thick shells, indicating that additional effects need to be considered in the structure of such complex core/shells. One possibility is that of inhomogeneous shell growth, namely that the shell is not growing evenly on all sides of the core. In addition, our simulation includes only planar stacking faults and does not include other kinds of defects at the core/shell interface. The structure of core/shells and the issues of lattice relaxation and surface reconstruction near the core/shell interface requires further study using more detailed structural probes such as X-ray absorption near-edge spectroscopy (XANES), which was recently used by Alivisatos and co-workers to study the surface disorder in InAs nanocrystals.[51] This is important, as defects such as dangling orbitals at the core/shell interface can serve as trap sites for the charge carriers and will limit the QY.

4. Model Calculations for the Band Gap. The core/shell band offsets provide control for modifying the electronic and optical properties of these composite nanocrystals. To examine the effect of the band offsets of various shells on the band gap of the composite nanocrystals, we performed calculations using a particle in a spherical box model as reported previously for other composite nanocrystals.[16,52] Briefly, in this model the electron and hole wave functions are treated separately, and the Coulombic interaction is then added within first-order perturbation theory.[53] Three radial potential regions should be considered in the core/shell nanocrystals: core, shell, and the surrounding organic layer. Continuity is required for the radial part of the wave functions for both electron and hole at the interfaces. In addition, the probability current, $1/m_i^*\ \mathrm{d}/\mathrm{d}r\ R_i(k_i r)$, where m_i^* is the effective mass in region i, R_i is the radial part of the lowest energy $1S_{e/h}$ electron or hole wave function, and k_i is the wave vector in region i, has to be continuous. We used the effective masses, and dielectric constants of the bulk semiconductors in the calculations.[41] The band offsets were taken from ref 30. First, for InAs cores, 1.7 nm in radius, we used a barrier height of 4.5 eV for the surrounding organic layer for both carriers. The confinement energy for the electron is sensitive to the barrier height because of the small electron effective mass, while the heavier hole is much less sensitive. The experimental value is in reasonable agreement with the calculated band gap, although there is a deviation, which is understandable in this simplistic model.[54] As the interesting value is the relative change of the band gap upon growth of the different shells, we plotted the calculated and measured shift in the band gap for various core/shells in Figure 10. The error in the band gap shifts should be

(50) Mann, B. *Acta Crystallogr.* **1968**, *A 24*, 321.
(51) Hamad, K. S.; Roth, R.; Rockenberger, J.; van Buuren, T.; Alivisatos, A. P. *Phys. Rev. Lett.* **1999**, *83*, 3474.
(52) Schoos, D.; Mews, A.; Eychmüller, A.; Weller, H. *Phys. Rev. B* **1994**, *49*, 17072.
(53) Brus, L. E. *J. Chem. Phys.* **1984**, *80*, 4403.
(54) Williamson, A. J.; Zunger, A. *Phys. Rev. B* **1999**, *59*, 15819.

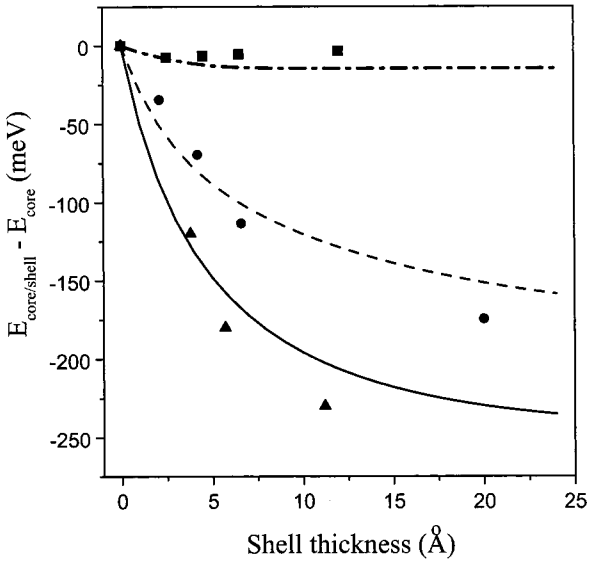

Figure 10. Experimental and calculated shifts of the band gap energy in various core/shells versus the shell thickness. InAs/ZnS core/shells: experimental data − squares, calculated shift of gap − dot−dashed line. InAs/InP core/shells: experimental data − circles, calculated shift of gap − dashed line. InAs/CdSe core/shells: experimental data − triangles, calculated shift of gap − solid line.

small compared with that in the absolute band gap energies. The agreement for the band gap shifts is good. For the ZnS shells (dot−dashed line), hardly any shift is observed both in the experiment and in the calculations. This is consistent with the large band offsets between InAs and ZnS. For both InP (dashed line) and CdSe (solid line) shells, the experimental and calculated band gaps shift to the red upon shell growth. This is due mainly to the reduction in the electron confinement energy in these core/shells. The lowest $1S_e$ level of the electron is above the core/shell barrier for both InP and CdSe shells leading to a high probability of presence of the electron in the shells.

5. Stability of Core/Shell Nanocrystals. Core/shell passivation with a shell of a semiconductor material that has large band offsets compared with the core, should provide increased protection and stability compared with the organically passivated core nanocrystals. We compared the photostability of the core/shells to IR140, a typical near-IR organic laser dye.[55] Solutions of nanocrystals and of the dye saturated with oxygen, were irradiated at 810 nm with a Ti−Sapphire laser for 30 min. An intensity of 250 mW was used, and the optical density of the irradiated solutions was 0.2 at 810 nm. Under these conditions, each nanocrystal and dye molecule absorbs a total of approximately 0.5×10^6 photons. For the dye, following the irradiation, the main absorption peak at 830 nm vanished, indicating that the dye completely degraded. For InAs cores (radius 1.7 nm), the absorption maximum shifted to the blue by 10 nm and the optical density slightly decreased. The PL intensity decreased by a factor of 2.1. For InAs/ZnSe core/shells (core radius 1.7 nm, shell thickness ~2 ML), the absorption did not change upon the irradiation, and the PL intensity decreased by a factor of 1.7, to a value still eight times stronger than for the fresh core. Finally, for InAs/CdSe core/shells (core radius 1.7 nm, shell thickness ~1.8 ML) the absorption shifted to the blue by 5 nm, and the PL intensity decreased by only 10%. This experiment demonstrates the improved photostability of the core/shells compared with a typical near-IR laser dye.

These core/shells also display greatly increased stability against oxidation compared with the cores. We studied the stability of the bare (TOP-coated) InAs cores, and the two core/shell samples similar to the ones examined above. We compared absorption and emission spectra of the fresh samples and of samples that were kept for 10 months in a solution saturated with oxygen under daylight conditions. The results are summarized in Figure 11. The InAs cores under these conditions exhibited a considerable blue-shift of the absorption accompanied by washing out of the spectral features. The emission was quenched by a factor of 40 compared with the fresh cores (Figure 11A). These phenomena indicate substantial oxidation of the bare cores. The core/shells under similar conditions show a very different behavior. For InAs/CdSe core/shells the absorption shifted slightly to the blue and the QY decreases from 16 to 13% (Figure 11B). Finally, for the InAs/ZnSe core/shells, the absorption hardly shifts and the emission QY is reduced from 19 to 15% (Figure 11C).

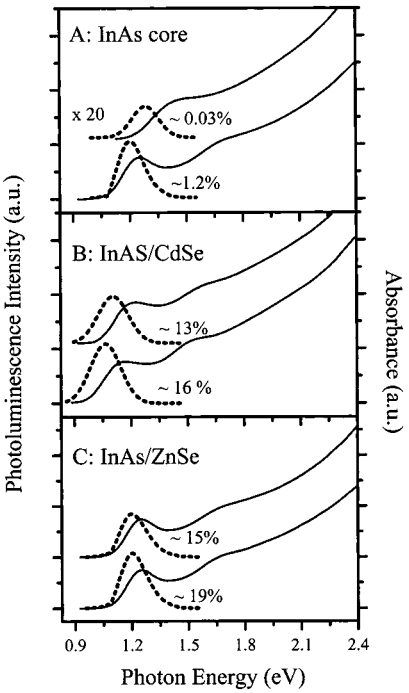

Figure 11. Comparison of stability of cores (frame A), InAs/CdSe core/shells (frame B), and InAs/ZnSe core/shells (frame C). Absorption spectra (solid lines) and PL spectra (dashed lines) are shown on the same energy scale for fresh (bottom traces in each frame), and for nanocrystals kept in an oxygen saturated solution for 10 months (top traces in each frame). The photoluminescence QY is also indicated in each case.

General Discussion

Following the successful synthesis of a variety of core/shell nanocrystals with InAs cores, using a broad range of core sizes, we can draw several insights on core/shell nanocrystals in general. We compare the chemistry and growth of II−VI versus III−V semiconductor core/shells. We then compare the core/shell colloidal growth with MBE growth of semiconductor quantum wells.

Core/shell nanocrystal synthesis should be controlled to allow shell growth while avoiding nucleation of nanocrystals of the shell material. In addition alloying is to be avoided while maintaining crystallinity and epitaxial growth. Finally, solubility of the core/shell nanocrystals has to be maintained. This requires careful control of critical parameters, which are the temperature, nanocrystal and solvent concentrations in the growth solution, and concentration and addition rate of the precursors. The

(55) Leduc, M.; Weisbuch, C. *Optics Commun.* **1978**, *26*, 78.

temperature is particularly critical for core/shells with InAs cores. The III−V semiconductor shells, in contrast to II−VI semiconductor shells, could only be grown at high temperatures because of the higher reaction barriers. We also found that even for the II−VI semiconductor shells, the higher temperature was needed for increasing the fluorescence QY. For shell growth at 260 °C, the maximum fluorescence QY of the products is ∼4 times larger than that obtained at 160 °C. In contrast, such lower temperatures were used to grow CdSe/CdS and CdSe/ZnS core/shells with high fluorescence QY.[14,15,16] The explanation to this interesting difference between core/shells with InAs and CdSe cores may be related to the different extent of ionic bonding in the two materials. The bonding in InAs, a III−V semiconductor, is less ionic than in CdSe, a II−VI semiconductor, and thus a higher temperature is needed to anneal defects, which trap the excited carriers at the core/shell interface. The inherent difference of the chemistry of the III−V versus the II−VI semiconductors may also explain why the maximum QY that we achieved in the core/shells with InAs cores was ∼20%, while for the CdSe/CdS and CdSe/ZnS higher yields, ranging between 30 and 90%, could be achieved.[14−16]

It is interesting to discuss further, the comparison between core/shell nanocrystals with InAs and CdSe cores. InAs/CdSe and CdSe/CdS core/shells are analogous in their electronic structure.[15] In both these cases, because of the relatively low conduction band offsets, the electron wave function extends to the shell and to the nanocrystal surface, and as a result the spectrum shifts red upon shell growth. Additionally, InAs/ZnSe and InAs/ZnS Core/shells are analogous to CdSe/ZnS nanocrystals.[14,16] Here, the band gap hardly changes upon shell growth, on account of the large band offsets between the core and the shell semiconductors.

The flexibility in the colloidal synthesis allowed us to grow a variety of shell materials using similar methodology. The II−VI semiconductor shell materials CdSe and ZnS generally adopted the cubic lattice of the InAs cores although in these same conditions, the nanocrystals of CdSe and ZnS form in wurtzite structure. The InAs core serves as a template with cubic structure for the shell growth. There have also been several reports of successful epitaxial growth of II−VI semiconductor materials on planar GaAs using MBE.[56]

The governing factor for growth mode in MBE is the lattice mismatch between the two semiconductors that build a nanostructure. Epitaxial layers can be grown if the lattice mismatch is small. With high lattice mismatch (higher than a few %), after deposition of a wetting layer, islands form spontaneously due to the strain.[57] In contrast, using colloidal synthesis it is possible to grow shells, even in cases of large lattice mismatch such as present for InAs/ZnSe, InAs/ZnS, InAs/GaAs, as well as for CdSe/ZnS. This difference arises from the small size of nanocrystals, which are smaller than the typical islands grown in MBE. However, strain also plays an important role in the colloidal grown core/shell nanocrystals, and may explain why the maximum QY is achieved for thin shells with thickness of 1−2 ML, as well as the general observation that further shell growth reduces the QY.

(56) Farrow, R. F. C.; Parkin, S. S. P.; Dobson, P. J.; Neave, J. H.; Arrott, A. S., Eds., *Thin Film Growth Techinques for Low-Dimensional Structures*; Plenum Press: New York, 1987.

(57) Leonard, D.; Krishnamurthy, M.; Reaves, C. M.; Denbaars, S. P.; Petroff, P. M. *Appl. Phys. Lett.* **1993**, *63*, 3203.

Conclusions

The synthesis of core/shell nanocrystals with InAs cores and a variety of shell materials was developed. A two-step high-temperature colloidal route was used, and the nanocrystals were characterized by a variety of methods. XPS provided direct proof that shells grow, and XRD data, supported by simulations, demonstrate that the growth mode is epitaxial for the crystalline shells even when II−VI semiconductor shells are grown. The simulations of the XRD patterns showed that on average, one stacking fault is present per 4−5 ML in both the core and the shells.

These core/shell nanocrystals exhibit a high emission QY tunable over the NIR spectral range, as well as increased stability against oxidation and photodegradation. Two tuning parameters were demonstrated for band gap engineering of core/shells. First, the core radius can be used to obtain InAs nanocrystals with band gaps covering a broad range of wavelengths between 800 and 1400 nm. Second, the choice of shell material modifies the electronic properties further. When growing ZnSe shells, the band gap energy is maintained because of the large band offsets, and emission QY as high as 20% could be achieved. Growing CdSe shells with smaller band offsets relative to InAs leads to a red-shift of the emission with enhancement of the QY also up to ∼20%. The ability to cover the NIR spectral range with high emission QY from the nanocrystals with enhanced stability suggests that they may be used as a novel type of fluorophore in this spectral region in which the selection of organic dyes is small and their stability is poor. The NIR emission is important in biological application as one can avoid the background fluorescence emanating from biomolecules, which lies in the visible range and overlaps with that of more conventional fluorophores. The emission from the novel InAs core/shells, by proper size tuning, can also cover the spectral range that is important for telecommunication applications.

Acknowledgment. We are indebted to Juanita Wickham for her assistance in the XRD simulations. We thank Dr. V. Soloviev, for help in the optical measurements, and Julia Aksenton, for assistance with the TEM studies. This research was supported in part by a grant from the Israel Academy of Sciences and Humanities, by a grant from the Binational US-Israel Science Foundation, and by a grant of the Israel Ministry of Science (Tastiot project). The Farkas Center for Light-Induced Processes is supported by the Minerva Gesellschaft für Forschung of the German Ministry for Research and Technology (BMFT). U.B thanks the Israeli Board of Higher Education for an Allon fellowship.

Supporting Information Available: Detailed synthetic procedure for preparation of the various core/shell compounds; table of dependence of QY on shell thickness for different preparations; figures with PL and absorption for two additional InAs/CdSe and InAs/ZnSe core/shells with 1.7 nm core radius (PDF). This material is available free of charge via the Internet at http://pubs.acs.org.

JA001386G